Bulletin of the Seismological Society of America, Vol. , No. , pp. –, , doi: 10.1785/0120180173

First Field Evidence of Coseismic Land-Level Change Associated with the 25 December 2016 M_w 7.6 Chiloé, Chile, Earthquake

by Ed Garrett, Martin Brader, Daniel Melnick,* Jonathan Bedford, and Diego Aedo

Abstract Assessments of megathrust earthquake rupture patterns provide fundamental insights into the processes that control the seismic cycle along subduction zones. When large earthquakes occur in regions with sparse geodetic networks, as was the case for the magnitude (M_w) 7.6 Chiloé, Chile, earthquake of 25 December 2016, estimates of vertical coseismic deformation from fixed intertidal biotic indicators provide important evidence that help to constrain fault slip. Ten months after the Chiloé earthquake, we observed a white fringe of bleached coralline algae (Corallinaceae) along the southeastern coastline of Isla Quilán, south of Isla de Chiloé, killed by reduced tidal wetting resulting from coseismic land uplift. Our quantitative measurements of the vertical extent of algal mortality provide the first field-based report of the effects of the 2016 earthquake. We infer Isla Quilán coseismically uplifted by 25.8 ± 14.3 cm. The vertical extent of mortality (VEM) and the aspect (compass direction) of the bedrock surface are uncorrelated, but we find that exposure to waves and shielding from insolation may prevent or delay mortality. Focusing on sites sheltered from waves, we demonstrate that with a large number of measurements (> 100), land-level changes as low as 25 cm may be quantitatively assessed. The absence of bleaching on Isla de Chiloé may reflect the smaller magnitude of coseismic uplift at this location or the lack of suitably sheltered bedrock surfaces. Previously published fault dislocation models are consistent with our field observations; however, the coralline algae data are on their own insufficient to discriminate between competing hypotheses over the amount of fault slip. By combining our field data with space geodetic data in a model that uses detailed fault geometry, we constrain peak slip to ~3 m, approximately 80% of the maximum cumulative plate convergence since the last great earthquake in the region.

Introduction

Assessing the slip distribution of megathrust earthquakes is fundamental to gain insight into the processes that control the seismic cycle. When megathrust earthquakes occur in regions with sparse geodetic networks, estimates of vertical coseismic deformation from fixed intertidal biotic indicators help constrain slip magnitudes and distributions (e.g., Plafker, 1965; Bodin and Klinger, 1986; Jaramillo *et al.*, 2012; Melnick *et al.*, 2012; Haeussler *et al.*, 2015). Even in areas with substantial geodetic coverage, uplift measurements based on biotic markers provide independent corroborative data at higher spatial densities than Global Positioning System (GPS) stations (e.g., Awata *et al.*, 2008; Clark *et al.*, 2017). The magnitude (M_w) 7.6 Chiloé earthquake (Fig. 1) ruptured the boundary between the Nazca and South American plates in the vicinity of the remote southern coast of Isla de Chiloé (~43.5° S), ending a period of seismic quiescence in the region stretching back to the 1960 $M_w < 9.5$ Valdivia earthquake, the largest instrumentally recorded earthquake globally. Inversion of seismic and Interferometric Synthetic Aperture Radar (InSAR) data provided initial outlines of the characteristics of the rupture, notably suggesting that the maximum coseismic slip of up to 5 m exceeded the slip deficit accumulated since 1960 (Lange *et al.*, 2017; Melgar *et al.*, 2017; Ruiz *et al.*, 2017; Xu, 2017). Subsequent integration of deformation recorded by continuous GPS stations—three within 100 km of the epicenter, but none overlying the rupture—suggested a lower maximum slip of ~2.9 m (Moreno *et al.*, 2018). Near-field observations from the epicentral region are critical for ground truthing these findings. The remote and predominantly offshore location of the rupture zone and the lack of a dense proximal geodetic network (Fig. 1) increase the importance of such observations.

*Also at Millennium Nucleus The Seismic Cycle Along Subduction Zones, Valdivia, Concepción, Valparaíso, Chile.

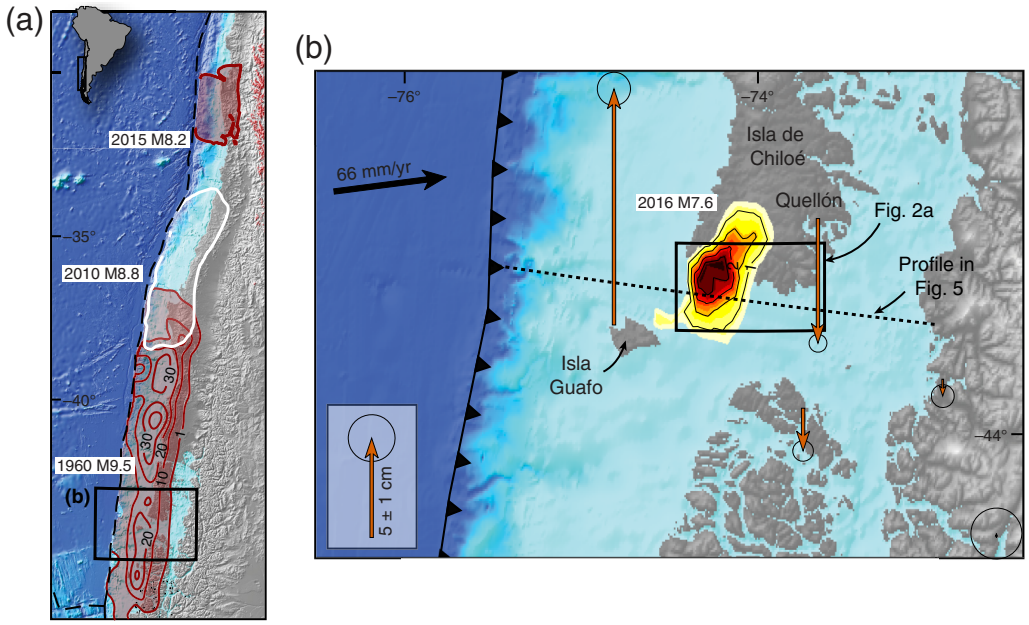

Figure 1. The regional context of the 2016 Chiloé earthquake. (a) The Chilean megathrust, including the slip distribution of the 1960 Valdivia earthquake, with contours in meters (Moreno *et al.*, 2009), and the location of the 2010 Maule and 2015 Illapel earthquakes. (b) The 2016 Chiloé earthquake including coseismic vertical Global Positioning System (GPS) offsets (arrows) and slip distribution in meters inferred from space-based geodesy (Moreno *et al.*, 2018). The color version of this figure is available only in the electronic edition.

In this article, we focus on quantitative estimates of coseismic land-level change provided by observations of sessile intertidal organisms. The use of fixed intertidal biota to determine the magnitude of abrupt vertical deformation is long established; members of the nineteenth century Her Majesty's Ship (HMS) Beagle expedition measured the $>$ 2 m width of a band of coseismically stranded mussels to assess the uplift of Isla Santa María during the 1835 M $>$ 8.5 Chilean earthquake (FitzRoy, 1839; Darwin, 1851). Increasingly, systematic approaches employed a range of intertidal flora and fauna to provide high-resolution reconstructions of abrupt changes in land level resulting from earthquakes (e.g., Tarr and Martin, 1912; Plafker, 1969; Plafker and Ward, 1992; Carver *et al.*, 1994; Meltzner *et al.*, 2010; Jaramillo *et al.*, 2017). Here, we focus on coralline algae, encrusting calcareous algae of the family Corallinaceae found at the lower limits of the intertidal range and subtidally within the photic zone (Ortlieb *et al.*, 1996). Our quantitative measurements of algal mortality provide the first field-based report of the effects of the 2016 earthquake. We seek to use our field observations to inform the debate regarding whether coseismic slip exceeded the post-1960 slip deficit and to understand the role of the 2016 earthquake within the seismic cycle of the Chilean megathrust.

Tectonic Setting and the 2016 Earthquake

The convergence of the Nazca and South American plates, at a rate of 66 mm yr^{-1} (Angermann *et al.*, 1999), drives the seismicity of the Chilean megathrust. Prior to the 2016 earthquake, the 1960 M_w 9.5 Valdivia rupture extended over an along-strike distance of ∼1000 km (Plafker and Savage, 1970), defining the extent of the Valdivia seismic segment (Fig. 1a). Moreno *et al.* (2009) inverted field estimates of coastal emergence and submergence derived by Plafker and Savage (1970) together with resurveyed triangulations and leveling lines to infer the distribution of slip in 1960, obtaining slip exceeding 25 m at the latitude of Isla Guafo, immediately southwest of Isla de Chiloé. GPS velocities collected between 2002 and 2009 suggest spatially heterogeneous post-1960 locking (Moreno *et al.*, 2011) with four highly locked regions distributed over the ∼1000−km−long rupture, including an area with a radius of approximately 50 km around Isla Guafo (43.6° S). The coincidence of this locked patch with the occurrence of high slip in 1960 suggests this asperity may be a persistent feature over several earthquake cycles (Moreno *et al.*, 2011).

The 2016 Chiloé earthquake occurred on the northeastern, down-dip flank of the interseismically locked Guafo patch, beneath the southern coast of Isla de Chiloé (Fig. 1b). Propagating from ∼15 km depth to the intersection between the subducting plate and the continental Moho (∼30 km), the rupture was confined to an area of approximately 15–20 km radius within the main seismogenic zone (Ruiz *et al.*, 2017; Moreno *et al.*, 2018). A lack of slip at shallow depths (seismogenic failure domains A and partly B, compare with fig. 15 in Lay *et al.*, 2012) precluded the generation of a tsunami; only small waves ($<$ 20 cm) were observed instrumentally. Inversions of geodetic and teleseismic data suggest peak slip between 2.9 (Moreno *et al.*, 2018) and 5.0 m (Melgar *et al.*, 2017), potentially exceeding the maximum accumulated slip deficit of ∼3.7 m implied by assuming full interseismic locking since 1960.

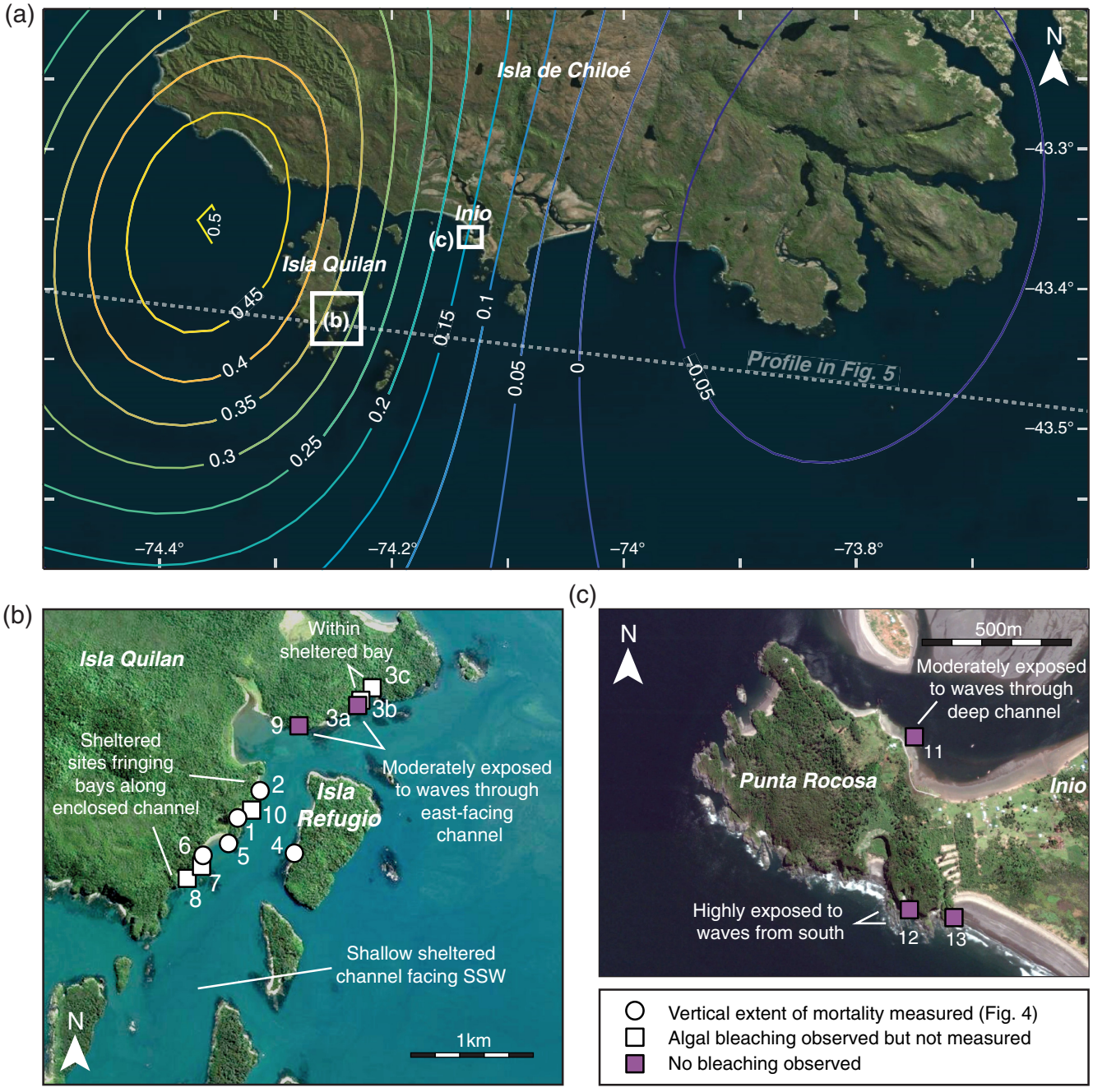

Figure 2. Field survey locations. (a) The southern coast of Isla de Chiloé and outlying islands. Contours indicate forward modeled coseismic vertical land-level change in 2016 resulting from inferred slip distribution of Moreno *et al.* (2018). Contours are at 0.05 m intervals, with uplift positive. (b) Coralline algae survey sites on the southeastern coast of Isla Quilán and the western coast of Isla Refugio. (c) Coralline algae survey sites around Punta Rocosa. The color version of this figure is available only in the electronic edition.

The area north of the 1960 Valdivia rupture zone was affected by the 2010 Maule earthquake (M 8.8), which had a rupture length of ~500 km (Moreno *et al.*, 2012). An analysis of surface displacements using continuous GPS stations spanning ~1000 km around the 2010 rupture shows an asymmetric rotation pattern and accelerated inland motion in two regions (Melnick *et al.*, 2017). These two regions coincided with locations of the 2015 Illapel (M_w 8.3, 30° S–32° S) and 2016 Chiloé earthquakes (Fig. 1a), leading Melnick *et al.* (2017) to interpret that the 2010 earthquake caused increased plate locking in these two regions during a superinterseismic phase.

Study Location

Our investigations focus on the southern coastline of Isla de Chiloé and the southeast of Isla Quilán (also known as Guapiquilán) (Fig. 2). Paleozoic and early Triassic

metamorphic rocks form the majority of central and southern Chiloé, with Tertiary volcanism locally exposed on Isla Quilán (Muñoz *et al.*, 2000; Duhart and Adriasola, 2008). The shorelines of southeastern Isla Quilán and the adjacent Isla Refugio possess exposed bedrock headlands and widespread sand, gravel, or boulder beaches (Fig. 2b). Adjacent to the settlement of Inio, the Río Inio estuary marks a center of Holocene fine-grained sedimentary accumulation. The rocky headland of Punta Rocosa lies at the mouth of the estuary (Fig. 2c). The remote location and very difficult access for much of the coastline prevented us from surveying other areas of southern Chiloé. The region of interest is microtidal, with a modeled great diurnal range of 1.56 m at Isla Quilán and 1.70 m at Punta Rocosa (Egbert and Erofeeva, 2002).

The bedrock outcrops and boulder accumulations around Isla Quilán and Punta Rocosa provide suitable environments for the development of sessile biotic communities. Although little published work relates to the southern coast of Chiloé, Velásquez *et al.* (2016) describe intertidal biota from analogous sites in northern Chiloé, 140–180 km north of the sites investigated in this article. They report 16 sessile taxa, but do not attempt to subdivide crustose coralline algae into different genera. Velásquez *et al.* (2016) report the greatest abundances of coralline algae—up to 100% coverage—in the lower middle and lower quartiles of the intertidal range. Co-occurring sessile taxa in the low intertidal zone include the cholorophyte *Codium dimorphum*, the branched coralline algae *Corallina officinalis* and the phaeophytes *Durvillaea antarctica* and *Lessonia spicata*.

The southern coastline of Chiloé lies within the zone of coseismic subsidence during the 1960 Valdivia earthquake (Fig. 1a). Comparison of the pre- and postearthquake lower growth limits of terrestrial vegetation suggests subsidence of 2.1 ± 0.2 m at the Quilanlar estuary, approximately 5 km east of Inio (Plafker and Savage, 1970). We observed ghost forests of dead but standing trees in locations now occupied by tidal marsh, tidal flat, or beach environments in the Inio estuary and on Isla Quilán, which we interpret as evidence of substantial relative sea level rise associated with coseismic subsidence in 1960. The living counterparts, a mixture of *Podocarpus nubigena*, *Sophora cassioides*, *Nothofagus dombeyi*, and species of the Myrtaceae family, are found above the highest reaches of current tides.

Field Approach

Lying above the rupture zone of the 2016 earthquake, southern Isla de Chiloé experienced coseismic vertical deformation on a centimeter to decimeter scale (Fig. 2a) (Lange *et al.*, 2017; Melgar *et al.*, 2017; Ruiz *et al.*, 2017; Xu, 2017). Coseismic uplift and subsidence were experienced along coastlines as abrupt decreases or increases in relative sea level. The direction, magnitude, and spatial pattern of these sea-level changes largely reflect the amount and distribution of slip on the fault (Thatcher, 1984; Nelson, 2007; Shennan *et al.*, 2016). Because the distribution of many sessile intertidal organisms along rocky coastlines closely reflects certain tidal levels, they may be used as precise and reliable indicators of current and past sea levels (Laborel and Laborel-Deguen, 1996; Laborel, 2005; Rovere *et al.*, 2015). Approaches for estimating coseismic uplift using sessile species predominantly focus on changes in the lethal limit, the elevation of the upper growth boundary above which the particular organism cannot survive (Kaye, 1964). When coseismically uplifted, organisms are raised above the lethal limit, resulting in mortality. The magnitude of uplift can consequently be derived through simply measuring the vertical extent of mortality (VEM), the difference in the upper limit of the dead organism and the upper limit of the living, postearthquake counterpart (Bodin and Klinger, 1986; Carver *et al.*, 1994).

Our field investigations, undertaken during low tides in August and October 2017, focused on identifying the upper limits of pre- and postearthquake coralline algae to establish the VEM. The crustose or rock encrusting forms of these calcareous red algae are widely distributed around the world, occurring from the lower limits of the intertidal zone down to the limit of the photic zone (Adey and Macintyre, 1973; Lagabrielle *et al.*, 2003). Their lethal limit is controlled by tidal inundation, with desiccation, elevated temperatures, and solar radiation resulting in the mortality of colonies that are exposed above water level for more than a few hours (Ortlieb *et al.*, 1996; Martone *et al.*, 2010). Mortality is accompanied by a characteristic color change from pink, purple, or light brown to white, with the bleached white colonies conspicuous for months after the bleaching event (e.g., Bodin and Klinger, 1986; Ramírez-Herrera and Orozco, 2002). The dead algae may be eroded over time by wave action, leading to underestimation of the magnitude of uplift if VEM measurements are not completed within months of the earthquake (Lagabrielle *et al.*, 2003). Postseismic deformation may also influence the distribution of the living postearthquake algae, with subsidence allowing recolonization of the lower margin of the bleached zone, further supporting the need for rapid assessments (Ramírez-Herrera and Orozco, 2002).

Our investigations of coralline algae in south central Chile follow their successful application for estimating coastal uplift associated with the 1995 Antofagasta earthquake (Ortlieb *et al.*, 1996), the 2010 Maule earthquake (Castilla *et al.*, 2010; Farías *et al.*, 2010; Vargas *et al.*, 2011), and the 2014 Iquique earthquake (Jaramillo *et al.*, 2017) in northern and central Chile. Ortlieb *et al.* (1996) and Vargas *et al.* (2011) note that the VEM is typically greater in locations more exposed to wave splash. Furthermore, uncertainty estimates are also greater for more exposed locations due to greater variability in the measured VEM (Vargas *et al.*, 2011). Vargas *et al.* (2011) suggest uncertainties of $\pm$10–20 cm for sheltered sites and $\pm$20–60 cm for areas highly exposed to waves. For each sampling site, we made a qualitative judgment on whether the site was sheltered, moderately exposed, or highly exposed to waves. We limited our measurements to bedrock sites with

largely parallel limits of the bleached and living algae colonies, avoiding detached blocks that could have moved during the earthquake. We also avoided areas with ponded water that might reduce or prevent desiccation. Cracks may enable wicking of water to higher elevations (Haeussler *et al.*, 2015), allowing isolated algae patches to survive at elevations above the main zone of encrustation. We avoided measuring these isolated patches, but note that the conglomeritic nature of the bedrock and the lack of smooth surfaces result in a degree of variability in the elevation of the upper limits of dead and living algae. By taking repeated VEM measurements at a horizontal spacing of 20–50 cm at sites with clearly defined limits, we sought to reduce this uncertainty.

Following Ramírez-Herrera and Orozco (2002), we measured the VEM along vertical surfaces using a tape measure. We report our measurements at the centimeter scale; however, the use of a tape measure introduces a small but unquantified uncertainty. Nevertheless, we assume that this uncertainty is not significant in comparison to the variability in the growth limits of the algae and in the consequent VEM. We report concurrent measurements of the aspect of the bedrock surface to the closest 10°.

Although Lemoine (1913, 1920) described four species from Isla de Chiloé, we do not attempt to classify the coralline algae encountered due to limited taxonomic analyses and difficulties in identification in the field (Meneses, 1993; Ortlieb *et al.*, 1996; Castilla *et al.*, 2010; Velásquez *et al.*, 2016).

Survey Results

We observed a laterally discontinuous band of bleached coralline algae visible at low tide during our two visits to Isla Quilán, eight and ten months after the 2016 Chiloé earthquake (Figs. 2b, 3a,b). Living algae at lower elevations beneath this white band retained their living brown or pink hue (Fig. 3c). During our second visit, in October 2017, we measured the VEM 103 times at five discrete but closely spaced sites in the southeast of Isla Quilán or the western coast of Isla Refugio (Fig. 2b, sites 1, 2, 4, 5, and 6). We noted the presence or absence of bleaching at a further seven sites on Isla Quilán (Fig. 2b, sites 3a, 3b, 3c, 7, 8, 9, and 10) and three more sites around Punta Rocosa at the mouth of the Inio estuary (Fig. 2c, sites 11, 12, and 13).

The mean VEM at the five Isla Quilán measurement sites ranged from 23.3 to 28.7 cm (Table 1). The mean of all 103 VEM measurements ($\pm 2\sigma$) was 25.8 ± 14.3 cm, with the data displaying a Gaussian distribution (Fig. 4a). At sites 3b, 3c, 7, 8, and 10, we observed bleaching but could not quantify the extent of mortality. Sites 3b, 3c, 8, and 10 lacked vertically inclined bedrock surfaces in which accurate measurements could be made; however, we observed bleaching on both subhorizontal bedrock outcrops and rounded boulders (Fig. 3e). Site 7 displayed bleached algae, but lacked clearly identifiable living algae, preventing us from ascertaining the postearthquake lethal limit.

We observed or measured bleaching at most aspects on Isla Quilán, with a notable exception between 150° and 210° (Fig. 4b). We do not find any relationship between the VEM and the aspect of the bedrock surface for aspects from 330° through to 90° ($r^2 = 0.001; n = 100$). Two moderately exposed south-facing sites on Isla Quilán (Fig. 2b, sites 3a, 9) displayed no bleaching, with pigmented and therefore presumably living algae at the highest extent of coralline algal growth (Fig. 3d). We did not observe any bleached algae at the three moderately or highly exposed sites around Punta Rocosa (Figs. 2c, 3f). These sites also share predominantly southerly aspects of 140°–200°.

Thresholds of Evidence Creation and Preservation

The absence of bleaching at sites 3a and 9 on Isla Quilán (Fig. 2b), despite the occurrence of bleaching at adjacent sites assumed to have experienced a similar magnitude of uplift, implies the existence of a threshold for bleaching that is not solely dependent on elevation with respect to the tidal frame. The two unbleached sites on Isla Quilán are moderately exposed to wave splash, and we propose that the combined effects of shielding from solar radiation due to their southern aspect, overhanging vegetation, and continued wetting may have prevented or delayed algal mortality. Although these environmental factors may exert a control on the presence or absence of bleaching, the extent to which they individually or in conjunction influence the magnitude of the VEM remains unclear. Our hypothesis that increased wave splash may contribute to preventing or delaying bleaching contrasts with previous investigations that suggest the VEM increases with increasing wave exposure (Ortlieb *et al.*, 1996; Vargas *et al.*, 2011), highlighting the need for further comprehensive assessments of the environmental controls on coralline algae bleaching.

Lagabrielle *et al.* (2003) highlight that subaerial erosion of the uppermost colonies of bleached algae may, over time, reduce the observed VEM. Their study of algae uplifted by the 1999 M_w 7.5 Ambrym earthquake, Vanuatu, notes lowering of the upper limit of bleached algae by several decimeters over 26 months following the earthquake, with near complete loss in some areas. We did not observe any evidence for erosion of bleached algae 10 months after the 2016 Chiloé earthquake; algae at the upper limit had been partially colonized by chlorophytes, but otherwise appeared intact and undamaged.

Postseismic deformation may influence the preservation of the magnitude of the coseismic uplift signal. Continued postseismic uplift may increase the VEM, whereas subsidence may allow recolonization of the lower margin of the bleached zone. Inverse modeling suggests maximum preearthquake interseismic uplift rates of 10 $\mathrm{mm\,yr^{-1}}$ at Isla Quilán (Melnick *et al.*, 2018). The extent to which this rate changed following the earthquake is unclear; however, earthquakes rupturing the deeper regions of the seismogenic zone have been characterized by short, low amplitude postseismic

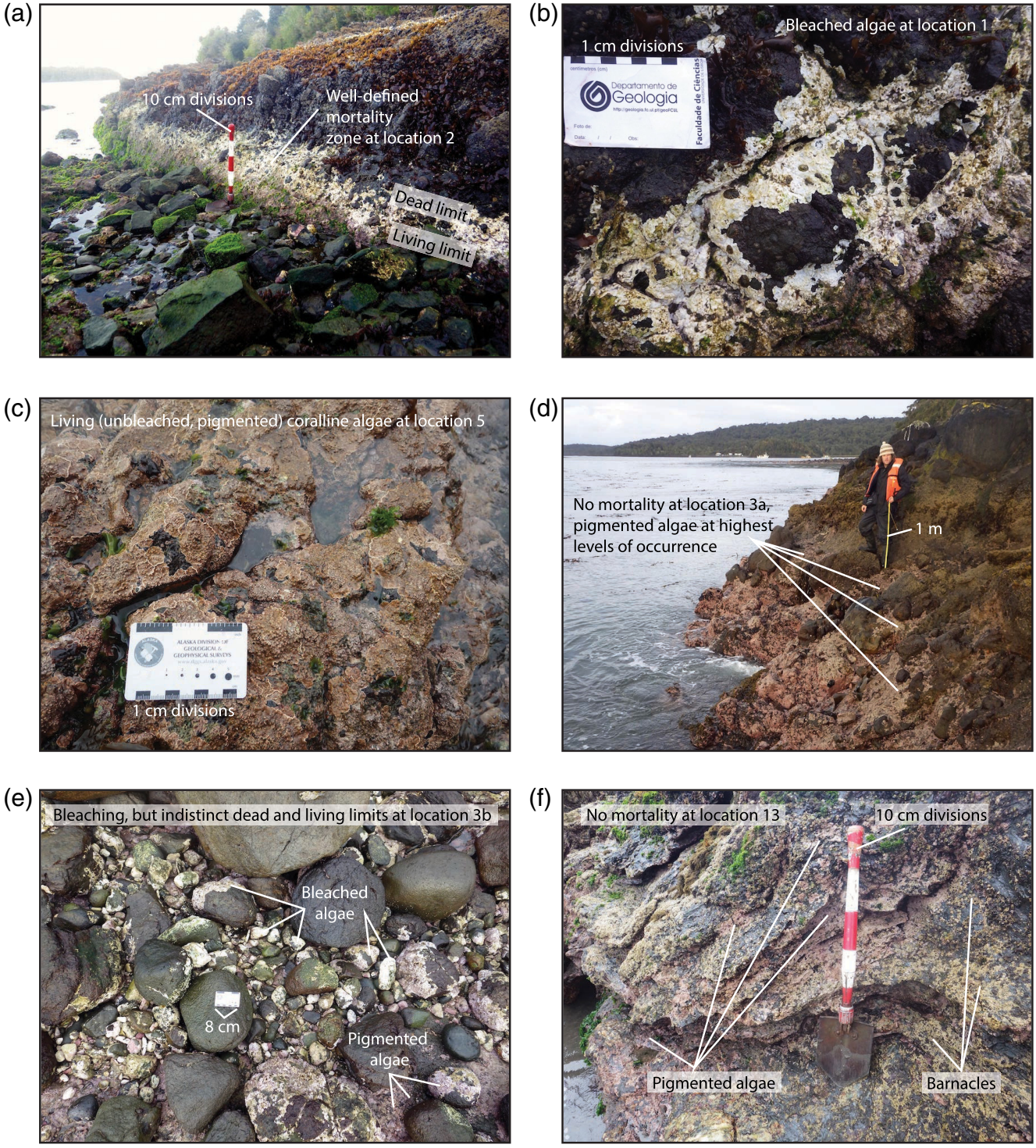

Figure 3. Field photographs of coralline algae survey sites on (a–e) Isla Quilán and (f) Punta Rocosa. (a,b) Conspicuous uplifted and bleached algae at sites 1 and 2. (c) Living algae at site 5 in an area with predominantly poorly defined growth limits. (d) Site 3a with no evidence of algal bleaching. (e) Site 3b displaying bleaching on mobile substrates and bedrock approximately 20 m from site 3a, but lacking vertically inclined surfaces suitable for vertical extent of mortality (VEM) measurement. (f) Living algae at site 13 in an area of low-surface coverage and poorly defined upper growth limits. The color version of this figure is available only in the electronic edition.

deformation (e.g., Béjar-Pizarro *et al.*, 2010; Melgar *et al.*, 2017). Therefore, the amplitude of postseismic deformation and the influence on the observed VEM might be limited. At Quellón (Fig. 1b), 70 mm of coseismic subsidence in 2016 was followed by 30 mm of postseismic uplift by October 2017 (Fig. 5). If Isla Quilán also experienced a reversal of the coseismic motion during the postseismic period, our VEM measurements may underestimate the magnitude of

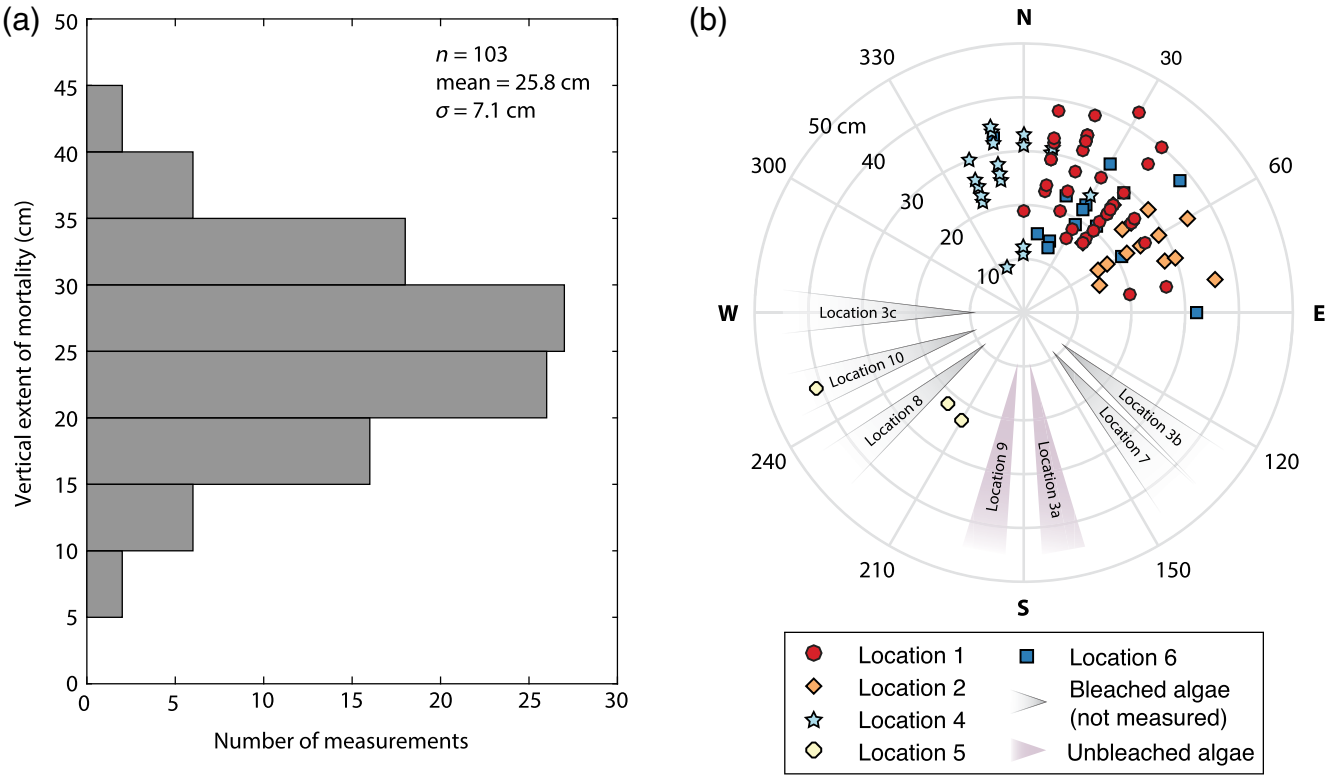

Figure 4. (a) Vertical extent of coralline algae mortality at Isla Quilán. (b) Rose diagram showing the aspect of sites with VEM measurements or observations of the presence or absence of bleaching. The color version of this figure is available only in the electronic edition.

Table 1
Summary of Coralline Algae Survey Data

Location	Site Number	Latitude (°)	Longitude (°)	Number of Measurements	Mean VEM (cm)	Standard Deviation (cm)	Mean Aspect (°)	Degree of Wave Exposure	Notes
Isla Quilán/ Isla Refugio	1	−43.41894	−74.25331	40	27.4	6.8	31	Sheltered	
	2	−43.41714	−74.25099	15	25.1	6.6	59	Sheltered	
	3a	−43.41095	−74.24069	–	–	–	170	Moderate	No bleaching observed
	3b	−43.41081	−74.24061	–	–	–	130	Sheltered	Bleaching evident but lacking vertical bedrock
	3c	−43.40992	−74.23958	–	–	–	270	Sheltered	Bleaching evident but lacking vertical bedrock
	4	−43.42138	−74.24784	26	25.3	7.5	352	Sheltered	
	5	−43.42107	−74.25425	3	28.7	10.7	227	Sheltered	Poorly defined growth limits in most areas
	6	−43.42155	−74.25694	19	23.3	7.1	35	Sheltered	
	7	−43.42225	−74.25701	–	–	–	140	Sheltered	Lacking clearly identifiable living algae
	8	−43.42325	−74.25905	–	–	–	230	Sheltered	Bleaching evident but lacking vertical bedrock
	9	−43.41234	−74.24683	–	–	–	190	Moderate	No bleaching observed
	10	−43.41834	−74.25217	–	–	–	250	Sheltered	Bleaching evident but lacking vertical bedrock
	Total			103	25.8	7.14			
Punta Rocosa, Isla de Chiloé	11	−43.36237	−74.13142	–	–	–	200	Moderate	No bleaching observed, poorly defined living limit
	12	−43.36757	−74.13046	–	–	–	160	High	No bleaching observed
	13	−43.36760	−74.12961	–	–	–	140	High	No bleaching observed, poorly defined living limit

See Table A1 for complete dataset. VEM, vertical extent of mortality.

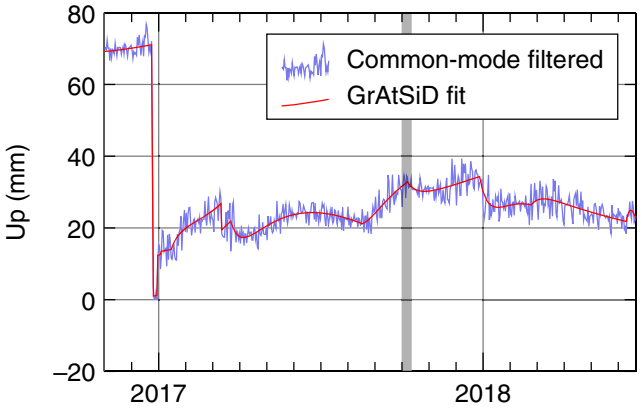

Figure 5. Coseismic and postseismic vertical displacements recorded by GPS station QLLN at Quellón (see Fig. 1b for location). We apply a common mode filter and model the time series with the GrAtSiD algorithm (Bedford and Bevis, 2018). The vertical bar indicates the timing of our VEM measurements at Isla Quilán in October 2017. The color version of this figure is available only in the electronic edition.

coseismic uplift due to subsequent subsidence. Nevertheless, if postseismic uplift at Quellón reflects afterslip down-dip of the mainshock, Isla Quilán may have experienced a smaller magnitude of postseismic subsidence, or continued uplift. As we currently have no further constraints on the postseismic deformation rate or direction, we cannot apply any straightforward correction to our VEM-based estimate of uplift.

Comparison with Slip Models

The vertical extent of coralline algae mortality suggests the 2016 Chiloé earthquake uplifted southeastern Isla Quilán by 25.8 ± 14.3 cm. In Figure 6, we compare this estimate with the vertical deformation predicted by dislocation models featuring either restricted peak slip (Moreno *et al.*, 2018) or peak slip exceeding the accumulated post-1960 slip deficit (Lange *et al.*, 2017). We project the Lange *et al.* (2017) slip distribution onto the more realistic, 3D, and undulating fault geometry of Moreno *et al.* (2018) to eliminate differences in surface deformation predictions resulting from this factor. This interpolation reduces the maximum slip in the Lange *et al.* (2017) model from 4.2 to 3.8 m, closer to the 3.7 m deficit implied by full locking, but still greater than the deficit that would be associated with incomplete or delayed post-1960 locking (Moreno *et al.*, 2011). Our field observations are consistent with either model, with both predicting uplift of between 20 and 35 cm at Isla Quilán. Predictions from both models highlight maximum uplift occurring trenchward, either ~10 or ~30 km west of Isla Quilán (Fig. 2a).

The lack of bleaching observed at Punta Rocosa suggests any coseismic uplift at this location did not exceed the evidence creation threshold. Our interpretation of the Isla Quilán observations suggests moderately exposed, south-facing colonies may remain unbleached even in the event of uplift of ~25 cm. As the Punta Rocosa sites are predominantly south facing and are moderately or highly exposed, we cannot rule out a small amount of uplift. Furthermore, Vargas *et al.* (2011) propose uncertainties in excess of ±20 cm for areas highly exposed to waves, providing additional evidence that these sites are not suited to recording centimeter-scale deformation. The models of both Lange *et al.* (2017) and Moreno *et al.* (2018) predict the hinge line between regions of uplift and subsidence lies to the east of Punta Rocosa, with the site having experienced uplift of 5–15 cm (Fig. 6).

Incorporating Field Data into Models of Coseismic Slip

Because our field observations are alone insufficient to discriminate between different slip models, we combine them with space-based geodetic data to constrain the distri-

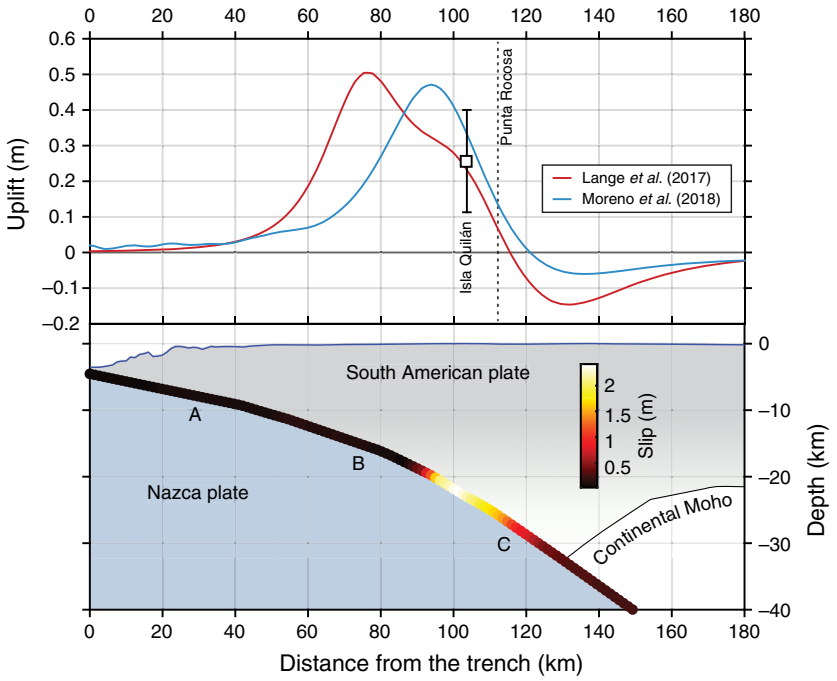

Figure 6. Predicted surface deformation (upper panel) resulting from Lange *et al.* (2017) and Moreno *et al.* (2018) slip distributions along the transect shown in Figure 1. Black box and whiskers represent uplift at Isla Quilán (VEM mean ±2σ). Both slip distributions use the fault geometry of Moreno *et al.* (2018), as shown in the lower panel. The lower panel also depicts slip distribution of Moreno *et al.* (2018) along the transect. Letters A, B, and C locate seismogenic failure domains (following Lay *et al.*, 2012). The color version of this figure is available only in the electronic edition.

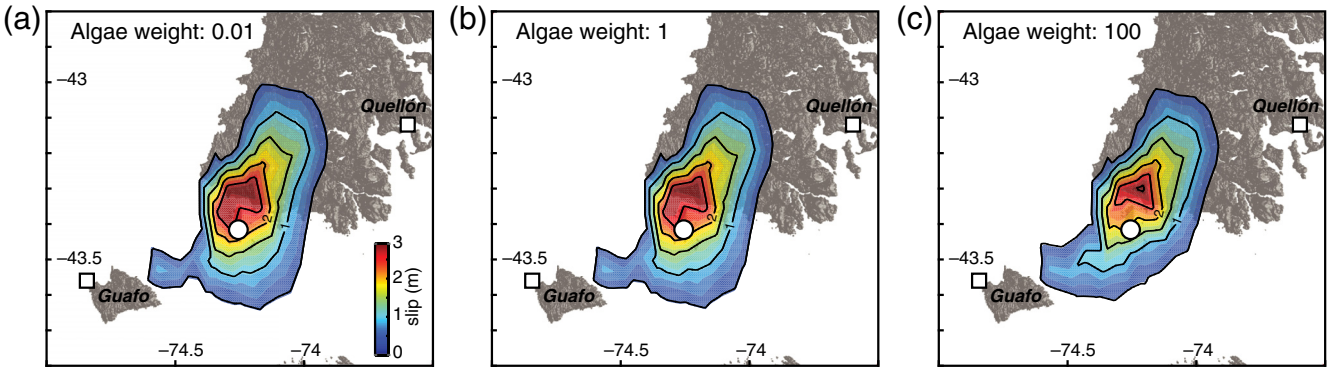

Figure 7. Impact of including the Isla Quilán uplift estimate (white circle) on the modeled distribution of coseismic fault slip in 2016. Initial model specifications are provided by Moreno *et al.* (2018), with the additional coralline algae constraint weighted at ratios of (a) 0.01:1, (b) 1:1, or (c) 100:1 with respect to the combined GPS and Interferometric Synthetic Aperture Radar (InSAR) data. White squares are GPS stations at Quellón and Guafo. The color version of this figure is available only in the electronic edition.

bution and magnitude of slip on the subduction interface. Because the initial GPS and InSAR-based model of Moreno *et al.* (2018) predict a similar magnitude of uplift at Isla Quilán to our VEM observations, incorporating and upweighting the VEM estimate as an additional constraint does not result in any appreciable revision to this slip model (Fig. 7). Joint inversion of coralline algae, GPS, and InSAR data indicates the rupture of a single asperity beneath the southern coast of Isla de Chiloé with maximum slip of ~3 m. Peak slip remains within 5% of 3 m as the coralline algae data are progressively more heavily weighted (Fig. 7). The heaviest weighting requires a modest (< 0.5 m) increase in slip to the southwest of Isla Quilán and a decrease in slip beneath and to the southeast of the island (Fig. 7c).

Discussion and Conclusions

Our field observations of sessile intertidal biota ground truth the amount of coseismic vertical deformation during the 2016 Chiloé earthquake. We interpret measurements of the VEM of crustose coralline algae to indicate Isla Quilán uplifted 25.8 ± 14.3 cm. We find no correlation between the VEM and the aspect of the bedrock surface, but note that exposure to waves and shielding from insolation due to aspect or overhanging vegetation may prevent or delay mortality. The lack of observed bleaching at Punta Rocosa on Isla de Chiloé may reflect the smaller magnitude of coseismic uplift and the lack of suitably sheltered sites. We find close agreement between our uplift estimate and the predictions of slip models developed using space-based geodetic and seismological approaches (Lange *et al.*, 2017; Moreno *et al.*, 2018). The agreement between our data and the modeling approaches provides further support for several aspects of this event previously noted by other authors. The Chiloé earthquake ruptured the deeper portion of the megathrust (Melgar *et al.*, 2017; Ruiz *et al.*, 2017; Xu, 2017; Moreno *et al.*, 2018), occurring toward the down-dip limit of a previously identified region of high-interseismic locking (Moreno *et al.*, 2011) and rerupturing an area that had experienced substantial coseismic slip (> 10 m) in 1960 (Moreno *et al.*, 2009). Rupture of the deeper regions of the interface (> 15 km) may reflect interseismic loading of this region by the strongly coupled shallower asperity (Moreno *et al.*, 2018).

Although earlier rupture models suggest coseismic slip in 2016 was greater than the ~3.7 m slip deficit accumulated since 1960 under the assumption of persistent decadal full locking (Lange *et al.*, 2017; Melgar *et al.*, 2017; Ruiz *et al.*, 2017; Xu, 2017), subsequent modeling implies lower peak slip and does not require exceedance of the slip deficit (Moreno *et al.*, 2018). Our incorporation of a coralline algae-based uplift estimate into the Moreno *et al.* (2018) model does not change this conclusion. Our modeled maximum slip of ~3 m constitutes approximately 80% of the cumulative plate convergence since the 1960 earthquake and would therefore be consistent with the release of all of the accumulated strain if plate coupling averaged 80% over this period. Nevertheless, we stress that the amount of coralline algae bleaching observed at Isla Quilán does not, in itself, preclude higher slip magnitudes and that these are a product of the fault geometry and geodetic data of Moreno *et al.* (2018). Models incorporating peak slip in excess of the maximum slip deficit also predict surface displacements within the uncertainty of our field observations (Lange *et al.*, 2017).

Our survey of coralline algae killed as a result of uplift during the 2016 Chiloé earthquake highlights the utility of these sessile intertidal organisms for providing quantitative coseismic deformation estimates in the absence of other near-field geodetic data. Our survey results and comparisons with published models demonstrate that with a large number of measurements (> 100) from closely spaced sites, land-level changes as low as 25 cm may be quantitatively assessed. Although sheltered sites provide consistent VEM estimates, the influence of wave splash on more exposed sites remains equivocal and further work is needed to evaluate the relative

importance of a range of environmental controls on coralline algae mortality in these situations.

Data and Resources

Observation of the tsunami wave height on 25 December 2016 is from the Puerto Melinka tide gauge, maintained by the Servicio Hidrográfico y Oceanográfico de la Armada de Chile and accessed via http://www.ioc-sealevelmonitoring.org/station.php?code=pmel. Global Positioning System (GPS) displacements in Figure 1 are from Moreno *et al.* (2018) and GPS time series in Figure 5 is from the Global Navigation Satellite Systems (GNSS) data repository of the Centro Sismologico Nacional, Chile (http://gps.csn.uchile.cl/data/). Basemaps in Figure 2 are from Google Earth version 7.3.1 (https://earth.google.com, image copyright DigitalGlobe 2018) and Bing Maps (https://www.bing.com/maps, image copyright Earthstar Geographics SIO 2018). Figure 7 uses Shuttle Radar Topography Mission (SRTM) data (U.S. Geological Survey [USGS], 2004) downloaded using the USGS EarthExplorer (https://earthexplorer.usgs.gov/). All websites were last accessed on September 2018. Figure 1 was drawn with the Generic Mapping Tools (Wessel *et al.*, 2013). All coralline algae data are provided in the Appendix.

Acknowledgments

This work was supported by the Natural Environment Research Council (NE/R00210X/1) with additional funding from the Department of Geography, Durham University. E.G. is funded by the European Union/Durham University (COFUND). The authors acknowledge financial support from the Millennium Nucleus CYCLO "The Seismic Cycle Along Subduction Zones" funded by the Millennium Scientific Initiative (ICM) of the Chilean Government Grant Number NC160025 and Chilean National Fund for Development of Science and Technology (FONDECYT) Grants Numbers 1150321 and 1181479. The authors thank Joaquim Otero for his help in the field, Dietrich Lange for providing his fault-slip model and Ian Shennan for comments on the article. The authors thank Aron Meltzner, an anonymous reviewer and Associate Editor Nicola Litchfield, for comments that improved the article. This is a contribution to International Geoscience Programme (IGCP) project 639.

References

Adey, W. H., and I. G. Macintyre (1973). Crustose coralline algae: A re-evaluation in the geological sciences, *Geol. Soc. Am. Bull.* **84,** 883–904.

Angermann, D., J. Klotz, and C. Reigber (1999). Space-geodetic estimation of the Nazca-South America Euler vector, *Earth Planet. Sci. Lett.* **171,** 329–334.

Awata, Y., S. Toda, H. Kaneda, T. Azuma, H. Horikawa, M. Shishikura, and T. Echigo (2008). Coastal deformation associated with the 2007 Noto Hanto earthquake, central Japan, estimated from uplifted and subsided intertidal organisms, *Earth Planets Space* **60,** 1059–1062.

Bedford, J., and M. Bevis (2018). Greedy automatic signal decomposition and its application to daily GPS time series, *J. Geophys. Res.* **123,** no. B014765, 6992–7003.

Béjar-Pizarro, M., D. Carrizo, A. Socquet, R. Armijo, S. Barrientos, F. Bondoux, S. Bonvalot, J. Campos, D. Comte, and J. B. De Chabalier (2010). Asperities and barriers on the seismogenic zone in North Chile: State-of-the-art after the 2007 M_w 7.7 Tocopilla earthquake inferred by GPS and InSAR data, *Geophys. J. Int.* **183,** 390–406.

Bodin, P., and T. Klinger (1986). Coastal uplift and mortality of intertidal organisms caused by the September 1985 Mexico earthquakes, *Science* **233,** 1071–1073.

Carver, G. A., A. S. Jayko, D. W. Valentine, and W. H. Li (1994). Coastal uplift associated with the 1992 Cape Mendocino earthquake, northern California, *Geology* **22,** 195–198.

Castilla, J. C., P. H. Manríquez, and A. Camaño (2010). Effects of rocky shore coseismic uplift and the 2010 Chilean mega-earthquake on intertidal biomarker species, *Mar. Ecol. Prog. Ser.* **418,** 17–23.

Clark, K. J., E. K. Nissen, J. D. Howarth, I. J. Hamling, J. J. Mountjoy, W. F. Ries, K. Jones, S. Goldstien, U. Cochran, and P. Villamor (2017). Highly variable coastal deformation in the 2016 M_w 7.8 Kaikōura earthquake reflects rupture complexity along a transpressional plate boundary, *Earth Planet. Sci. Lett.* **474,** 334–344.

Darwin, C. (1851). *Geological Observations on Coral Reefs, Volcanic Islands, and on South America: Being the Geology of the Voyage of the Beagle, under the Command of Captain Fitzroy, RN, during the Years 1832 to 1836*, Smith, Elder and Co., London, United Kingdom.

Duhart, P., and A. C. Adriasola (2008). New time-constraints on provenance, metamorphism and exhumation of the Bahía Mansa metamorphic complex on the Main Chiloé Island, south-central Chile, *Andean Geol.* **35,** 79–104.

Egbert, G. D., and S. Y. Erofeeva (2002). Efficient inverse modeling of barotropic ocean tides, *J. Atmos. Ocean. Technol.* **19,** 183–204.

Farías, M., G. Vargas, A. Tassara, S. Carretier, S. Baize, D. Melnick, and K. Bataille (2010). Land-level changes produced by the M_w 8.8 2010 Chilean earthquake, *Science* **329,** 916.

FitzRoy, R. (1839). *Narrative of the Surveying Voyages of His Majesty's Ships Adventure and Beagle between the Years 1826 and 1836: Describing their Examination of the Southern Shores of South America, and the Beagle's Circumnavigation of the Globe*, Henry Colburn, London, United Kingdom.

Haeussler, P. J., R. C. Witter, and K. Wang (2015). Intertidal biological indicators of coseismic subsidence during the M_w 7.8 Haida Gwaii, Canada, earthquake, *Bull. Seismol. Soc. Am.* **105,** 1265–1279.

Jaramillo, E., J. E. Dugan, D. M. Hubbard, D. Melnick, M. Manzano, C. Duarte, C. Campos, and R. Sanchez (2012). Ecological implications of extreme events: Footprints of the 2010 earthquake along the Chilean coast, *PLoS One* **7,** e35348, doi: 10.1371/journal.pone.0035348.

Jaramillo, E., D. Melnick, J. C. Baez, H. Montecino, N. A. Lagos, E. Acuña, M. Manzano, and P. A. Camus (2017). Calibrating coseismic coastal land-level changes during the 2014 Iquique (M_w = 8.2) earthquake (northern Chile) with leveling, GPS and intertidal biota, *PLoS One* **12,** e0174348, doi: 10.1371/journal.pone.0174348.

Kaye, C. A. (1964). The upper limit of barnacles as an index of sea-level change on the New England coast during the past 100 years, *J. Geol.* **72,** 580–600.

Laborel, J. (2005). Algal rims, in *Encyclopedia of Coastal Science*, M. Schwartz (Editor), Wiley, New York, New York, 24–25.

Laborel, J., and F. Laborel-Deguen (1996). Biological indicators of Holocene sea-level and climatic variations on rocky coasts of tropical and subtropical regions, *Quaternary Int.* **31,** 53–60.

Lagabrielle, Y., B. Pelletier, G. Cabioch, M. Régnier, and S. Calmant (2003). Coseismic and long-term vertical displacement due to back arc shortening, central Vanuatu: Offshore and onshore data following the M_w 7.5, 26 November 1999 Ambrym earthquake, *J. Geophys. Res.* **108,** no. B11, 2519.

Lange, D., J. Ruiz, S. Carrasco, and P. Manríquez (2017). The Chiloé M_w 7.6 earthquake of 25 December 2016 in Southern Chile and its relation to the M_w 9.5 1960 Valdivia earthquake, *Geophys. J. Int.* **213,** 210–221.

Lay, T., H. Kanamori, C. J. Ammon, K. D. Koper, A. R. Hutko, L. Ye, H. Yue, and T. M. Rushing (2012). Depth-varying rupture properties of subduction zone megathrust faults, *J. Geophys. Res.* **117,** no. B04311, doi: 10.1029/2011JB009133.

Lemoine, P. (1913). Mélobésiées, in *Deuxième Expédition Antarctique Française (1908–1910)*, J. Charcot and L. Joubin (Editors), Masson and Cie, Paris, France, 1–67 (in French).

Lemoine, P. (1920). Botanische Ergebnisse der schwedischen Expedition nach Patagonien und dem Feuerlande 1907–1909, VII. Melobésiés, *K. Sven. Vetenskapsakademiens Handl.* **61,** 1–17 (in German).

Martone, P. T., M. Alyono, and S. Stites (2010). Bleaching of an intertidal coralline alga: Untangling the effects of light, temperature, and desiccation, *Mar. Ecol. Prog. Ser.* **416,** 57–67.

Melgar, D., S. Riquelme, X. Xu, J. C. Baez, J. Geng, and M. Moreno (2017). The first since 1960: A large event in the Valdivia segment of the Chilean Subduction Zone, the 2016 M7.6 Melinka earthquake, *Earth Planet. Sci. Lett.* **474,** 68–75.

Melnick, D., M. Cisternas, M. Moreno, and R. Norambuena (2012). Estimating coseismic coastal uplift with an intertidal mussel: Calibration for the 2010 Maule Chile earthquake (M_w = 8.8), *Quaternary Sci. Rev.* **42,** 29–42.

Melnick, D., S. Li, M. Moreno, M. Cisternas, J. Jara-Muñoz, R. Wesson, A. Nelson, J. C. Báez, and Z. Deng (2018). Back to full interseismic plate locking decades after the giant 1960 Chile earthquake, *Nat. Commun.* **9,** no. 3527, doi: 10.1038/s41467-018-05989-6.

Melnick, D., M. Moreno, J. Quinteros, J. C. Baez, Z. Deng, S. Li, and O. Oncken (2017). The super-interseismic phase of the megathrust earthquake cycle in Chile, *Geophys. Res. Lett.* **44,** 784–791.

Meltzner, A. J., K. Sieh, H. Chiang, C. Shen, B. W. Suwargadi, D. H. Natawidjaja, B. E. Philibosian, R. W. Briggs, and J. Galetzka (2010). Coral evidence for earthquake recurrence and an A.D. 1390–1455 cluster at the south end of the 2004 Aceh–Andaman rupture, *J. Geophys. Res.* **115,** no. B10402, doi: 10.1029/2010JB007499.

Meneses, I. C. (1993). Vertical distribution of coralline algae in the rocky intertidal of northern Chile, *Proc. of the Fourteenth International Seaweed Symposium*, A. R. O Chapman, M. T. Brown, and M. Lahaye (Editors) Springer, Dordrecht, The Netherlands, 121–129.

Moreno, M., S. Li, D. Melnick, J. R. Bedford, J. C. Baez, M. Motagh, S. Metzger, S. Vajedian, C. Sippl, and B. D. Gutknecht (2018). Chilean megathrust earthquake recurrence linked to frictional contrast at depth, *Nature Geosci.* **11,** 285.

Moreno, M., D. Melnick, M. Rosenau, J. C. Baez, J. Klotz, O. Oncken, A. Tassara, J. Chen, K. Bataille, and M. Bevis (2012). Toward understanding tectonic control on the M_w 8.8 2010 Maule Chile earthquake, *Earth Planet. Sci. Lett.* **321,** 152–165.

Moreno, M., D. Melnick, M. Rosenau, J. Bolte, J. Klotz, H. Echtler, J. C. Baez, K. Bataille, J. Chen, and M. Bevis (2011). Heterogeneous plate locking in the South–Central Chile subduction zone: Building up the next great earthquake, *Earth Planet. Sci. Lett.* **305,** 413–424.

Moreno, M. S., J. Bolte, J. Klotz, and D. Melnick (2009). Impact of megathrust geometry on inversion of coseismic slip from geodetic data: Application to the 1960 Chile earthquake, *Geophys. Res. Lett.* **36,** L16310, doi: 10.1029/2009GL039276.

Muñoz, J., R. Troncoso, P. Duhart, P. Crignola, L. Farmer, and C. R. Stern (2000). The relation of the mid-Tertiary coastal magmatic belt in south-central Chile to the late Oligocene increase in plate convergence rate, *Rev. Geológica Chile* **27,** 177–203.

Nelson, A. R. (2007). Tectonic locations, in *Encylopedia of Quaternary Science*, S. A. Elias (Editor), Elsevier, Amsterdam, The Netherlands, 3072–3087.

Ortlieb, L., S. Barrientos, and N. Guzman (1996). Coseismic coastal uplift and coralline algae record in northern Chile: The 1995 Antofagasta earthquake case, *Quaternary Sci. Rev.* **15,** 949–960.

Plafker, G. (1965). Tectonic deformation associated with the 1964 Alaska earthquake, *Science* **148,** 1675–1687.

Plafker, G. (1969). *Tectonics of the March 27, 1964, Alaska earthquake*, U.S. Government Printing Office, Washington, D.C.

Plafker, G., and J. C. Savage (1970). Mechanism of the Chilean earthquakes of May 21 and 22, 1960, *Geol. Soc. Am. Bull.* **81,** 1001–1030.

Plafker, G., and S. N. Ward (1992). Back-arc thrust faulting and tectonic uplift along the Caribbean Sea coast during the April 22, 1991, Costa Rica earthquake, *Tectonics* **11,** 709–718.

Ramírez-Herrera, M.-T., and J. J. Z. Orozco (2002). Coastal uplift and mortality of coralline algae caused by a 6.3 M_w earthquake, Oaxaca, Mexico, *J. Coastal Res.* **18,** 75–81.

Rovere, A., F. Antonioli, and C. N. Bianchi (2015). Fixed biological indicators, in *Handbook of Sea-Level Research*, I. Shennan, A. J. Long, and B. P. Horton (Editors), Wiley, Hoboken, New Jersey, 268–280.

Ruiz, S., M. Moreno, D. Melnick, F. Campo, P. Poli, J. C. Baez, F. Leyton, and R. Madariaga (2017). Reawakening of large earthquakes in South-Central Chile: The 2016 M_w7. 6 Chiloé event, *Geophys. Res. Lett.* **44,** 6633–6640.

Shennan, I., E. Garrett, and N. Barlow (2016). Detection limits of tidal-wetland sequences to identify variable rupture modes of megathrust earthquakes, *Quaternary Sci. Rev.* **150,** 1–30.

Tarr, R. S., and L. Martin (1912). The earthquakes at Yakutat Bay, Alaska, in September, 1899, *Bull. Seismol. Soc. Am.* **2,** 254–255.

Thatcher, W. (1984). The earthquake deformation cycle at the Nankai Trough, southwest Japan, *J. Geophys. Res.* **89,** 3087–3101.

U.S. Geological Survey (USGS) (2004). *Shuttle Radar Topography Mission*, 1 Arc Second scenes s44_w075, s44_w074, s43_w075 and s43_074, Unfilled Unfinished 2.0, Global Land Cover Facility, University of Maryland, College Park, Maryland, February 2000.

Vargas, G., M. Farías, S. Carretier, A. Tassara, S. Baize, and D. Melnick (2011). Coastal uplift and tsunami effects associated to the 2010 M_w 8. 8 Maule earthquake in Central Chile, *Andean Geol.* **38,** 219–238.

Velásquez, C., E. Jaramillo, P. A. Camus, M. Manzano, and R. Sánchez (2016). Biota del intermareal rocoso expuesto de la Isla Grande de Chiloé, Archipiélago de Chiloé, Chile: Patrones de diversidad e implicancias ecológicas y biogeográficas, *Rev. Biol. Mar. Oceanogr.* **51,** 33–50.

Wessel, P., W. H. F. Smith, R. Scharroo, J. F. Luis, and F. Wobbe (2013). Generic mapping tools: Improved version released, *EOS Trans. AGU* **94,** 409–410.

Xu, W. (2017). Finite-fault Slip Model of the 2016 M_w 7.5 Chiloé earthquake, Southern Chile, estimated from Sentinel-1 data, *Geophys. Res. Lett.* **44,** 4774–4780.

Appendix

Table A1 provides the complete list of coralline algae measurements, summarized in Table 1, for each of the measurement points on Isla Quilán and Isla Refugio.

Table A1

Vertical Extent of Coralline Algae Mortality and Corresponding Bedrock Surface Aspect for Each Measurement Point

SITE	VEM (CM)	ASPECT (°)
1	39	20
1	29	10
1	23	10
1	32	10
1	19	0
1	26	60
1	28	20
1	34	20
1	35	20
1	38	10
1	26	40
1	29	10
1	43	30
1	29	40
1	40	40
1	35	20
1	18	40
1	20	40

(*continued*)

Table A1 (*Continued*)

SITE	VEM (CM)	ASPECT (°)
1	24	40
1	24	20
1	25	40
1	18	30
1	26	50
1	27	80
1	32	20
1	33	10
1	17	40
1	29	30
1	26	40
1	34	20
1	36	40
1	22	20
1	22	40
1	24	40
1	24	10
1	20	40
1	25	40
1	16	30
1	20	80
1	27	50
2	36	80
2	35	60
2	30	70
2	28	70
2	25	60
2	26	50
2	29	60
2	30	50
2	22	60
2	18	60
2	16	60
2	17	40
2	24	50
2	26	40
2	15	70
4	25	350
4	23	340
4	32	30
4	30	340
4	32	350
4	22	340
4	26	350
4	30	10
4	33	0
4	34	350
4	23	340
4	9	340
4	11	0
4	35	350
4	25	340
4	25	30
4	30	340
4	28	350
4	26	340
4	26	350
4	31	10
4	31	0
4	28	350
4	23	340
4	9	340
4	12	0
5	22	220
5	41	250
5	23	210
6	32	90
6	30	70
6	38	50
6	22	30
6	32	30
6	17	40
6	29	40
6	23	20
6	21	60
6	19	30
6	21	40
6	19	30
6	23	30
6	19	30
6	15	10
6	33	350
6	14	20
6	23	30
6	13	20

VEM, vertical extent of mortality.

Department of Geography
Durham University
South Road
Durham DH1 3LE, United Kingdom
edmund.garrett@durham.ac.uk
(E.G., M.B.)

Instituto de Ciencias de la Tierra
TAQUCh
Universidad Austral de Chile
Valdivia 511430, Chile
(D.M., D.A.)

GFZ German Research Centre for Geosciences
Telegrafenberg, Building C
14473 Potsdam, Germany
(J.B.)

Manuscript received 25 June 2018